

Updated measurements of the M1 transition $\psi(3686) \rightarrow \gamma\eta_c(2S)$ with $\eta_c(2S) \rightarrow K\bar{K}\pi$

M. Ablikim,¹ M. N. Achasov,^{5,b} P. Adlarson,⁷⁵ X. C. Ai,⁸¹ R. Aliberti,³⁶ A. Amoroso,^{74a,74c} M. R. An,⁴⁰ Q. An,^{71,58} Y. Bai,⁵⁷ O. Bakina,³⁷ I. Balossino,^{30a} Y. Ban,^{47,g} V. Batozskaya,^{1,45} K. Begzsuren,³³ N. Berger,³⁶ M. Berlowski,⁴⁵ M. Bertani,^{29a} D. Bettoni,^{30a} F. Bianchi,^{74a,74c} E. Bianco,^{74a,74c} A. Bortone,^{74a,74c} I. Boyko,³⁷ R. A. Briere,⁶ A. Brueggemann,⁶⁸ H. Cai,⁷⁶ X. Cai,^{1,58} A. Calcaterra,^{29a} G. F. Cao,^{1,63} N. Cao,^{1,63} S. A. Cetin,^{62a} J. F. Chang,^{1,58} T. T. Chang,⁷⁷ W. L. Chang,^{1,63} G. R. Che,⁴⁴ G. Chelkov,^{37,a} C. Chen,⁴⁴ Chao Chen,⁵⁵ G. Chen,¹ H. S. Chen,^{1,63} M. L. Chen,^{1,58,63} S. J. Chen,⁴³ S. L. Chen,⁴⁶ S. M. Chen,⁶¹ T. Chen,^{1,63} X. R. Chen,^{32,63} X. T. Chen,^{1,63} Y. B. Chen,^{1,58} Y. Q. Chen,³⁵ Z. J. Chen,^{26,h} W. S. Cheng,^{74c} S. K. Choi,¹¹ X. Chu,⁴⁴ G. Cibinetto,^{30a} S. C. Coen,⁴ F. Cossio,^{74c} J. J. Cui,⁵⁰ H. L. Dai,^{1,58} J. P. Dai,⁷⁹ A. Dbeysi,¹⁹ R. E. de Boer,⁴ D. Dedovich,³⁷ Z. Y. Deng,¹ A. Denig,³⁶ I. Denysenko,³⁷ M. Destefanis,^{74a,74c} F. De Mori,^{74a,74c} B. Ding,^{66,1} X. X. Ding,^{47,g} Y. Ding,³⁵ Y. Ding,⁴¹ J. Dong,^{1,58} L. Y. Dong,^{1,63} M. Y. Dong,^{1,58,63} X. Dong,⁷⁶ M. C. Du,¹ S. X. Du,⁸¹ Z. H. Duan,⁴³ P. Egorov,^{37,a} Y. H. Fan,⁴⁶ J. Fang,^{1,58} S. S. Fang,^{1,63} W. X. Fang,¹ Y. Fang,¹ R. Farinelli,^{30a} L. Fava,^{74b,74c} F. Feldbauer,⁴ G. Felici,^{29a} C. Q. Feng,^{71,58} J. H. Feng,⁵⁹ K. Fischer,⁶⁹ M. Fritsch,⁴ C. D. Fu,¹ J. L. Fu,⁶³ Y. W. Fu,¹ H. Gao,⁶³ Y. N. Gao,^{47,g} Yang Gao,^{71,58} S. Garbolino,^{74c} I. Garzia,^{30a,30b} P. T. Ge,⁷⁶ Z. W. Ge,⁴³ C. Geng,⁵⁹ E. M. Gersabeck,⁶⁷ A. Gilman,⁶⁹ K. Goetzen,¹⁴ L. Gong,⁴¹ W. X. Gong,^{1,58} W. Gradl,³⁶ S. Gramigna,^{30a,30b} M. Greco,^{74a,74c} M. H. Gu,^{1,58} Y. T. Gu,¹⁶ C. Y. Guan,^{1,63} Z. L. Guan,²³ A. Q. Guo,^{32,63} L. B. Guo,⁴² M. J. Guo,⁵⁰ R. P. Guo,⁴⁹ Y. P. Guo,^{13,f} A. Guskov,^{37,a} T. T. Han,⁵⁰ W. Y. Han,⁴⁰ X. Q. Hao,²⁰ F. A. Harris,⁶⁵ K. K. He,⁵⁵ K. L. He,^{1,63} F. H. H. Heinsius,⁴ C. H. Heinz,³⁶ Y. K. Heng,^{1,58,63} C. Herold,⁶⁰ T. Holtmann,⁴ P. C. Hong,^{13,f} G. Y. Hou,^{1,63} X. T. Hou,^{1,63} Y. R. Hou,⁶³ Z. L. Hou,¹ H. M. Hu,^{1,63} J. F. Hu,^{56,i} T. Hu,^{1,58,63} Y. Hu,¹ G. S. Huang,^{71,58} K. X. Huang,⁵⁹ L. Q. Huang,^{32,63} X. T. Huang,⁵⁰ Y. P. Huang,¹ T. Hussain,⁷³ N. Hüsken,^{28,36} N. in der Wiesche,⁶⁸ M. Irshad,^{71,58} J. Jackson,²⁸ S. Jaeger,⁴ S. Janchiv,³³ J. H. Jeong,¹¹ Q. Ji,¹ Q. P. Ji,²⁰ X. B. Ji,^{1,63} X. L. Ji,^{1,58} Y. Y. Ji,⁵⁰ X. Q. Jia,⁵⁰ Z. K. Jia,^{71,58} H. J. Jiang,⁷⁶ P. C. Jiang,^{47,g} S. S. Jiang,⁴⁰ T. J. Jiang,¹⁷ X. S. Jiang,^{1,58,63} Y. Jiang,⁶³ J. B. Jiao,⁵⁰ Z. Jiao,²⁴ S. Jin,⁴³ Y. Jin,⁶⁶ M. Q. Jing,^{1,63} T. Johansson,⁷⁵ X. K.,¹ S. Kabana,³⁴ N. Kalantar-Nayestanaki,⁶⁴ X. L. Kang,¹⁰ X. S. Kang,⁴¹ M. Kavatsyuk,⁶⁴ B. C. Ke,⁸¹ A. Khoukaz,⁶⁸ R. Kiuchi,¹ R. Kliemt,¹⁴ O. B. Kolcu,^{62a} B. Kopf,⁴ M. Kuessner,⁴ A. Kupsc,^{45,75} W. Kühn,³⁸ J. J. Lane,⁶⁷ P. Larin,¹⁹ A. Lavania,²⁷ L. Lavezzi,^{74a,74c} T. T. Lei,^{71,58} Z. H. Lei,^{71,58} H. Leithoff,³⁶ M. Lellmann,³⁶ T. Lenz,³⁶ C. Li,⁴⁴ C. Li,⁴⁸ C. H. Li,⁴⁰ Cheng Li,^{71,58} D. M. Li,⁸¹ F. Li,^{1,58} G. Li,¹ H. Li,^{71,58} H. B. Li,^{1,63} H. J. Li,²⁰ H. N. Li,^{56,i} Hui Li,⁴⁴ J. R. Li,⁶¹ J. S. Li,⁵⁹ J. W. Li,⁵⁰ K. L. Li,²⁰ Ke Li,¹ L. J. Li,^{1,63} L. K. Li,¹ Lei Li,³ M. H. Li,⁴⁴ P. R. Li,^{39,j,k} Q. X. Li,⁵⁰ S. X. Li,¹³ T. Li,⁵⁰ W. D. Li,^{1,63} W. G. Li,¹ X. H. Li,^{71,58} X. L. Li,⁵⁰ Xiaoyu Li,^{1,63} Y. G. Li,^{47,g} Z. J. Li,⁵⁹ Z. X. Li,¹⁶ C. Liang,⁴³ H. Liang,^{1,63} H. Liang,³⁵ H. Liang,^{71,58} Y. F. Liang,⁵⁴ Y. T. Liang,^{32,63} G. R. Liao,¹⁵ L. Z. Liao,⁵⁰ Y. P. Liao,^{1,63} J. Libby,²⁷ A. Limphirat,⁶⁰ D. X. Lin,^{32,63} T. Lin,¹ B. J. Liu,¹ B. X. Liu,⁷⁶ C. Liu,³⁵ C. X. Liu,¹ F. H. Liu,⁵³ Fang Liu,¹ Feng Liu,⁷ G. M. Liu,^{56,i} H. Liu,^{39,j,k} H. B. Liu,¹⁶ H. M. Liu,^{1,63} Huanhuan Liu,¹ Huihui Liu,²² J. B. Liu,^{71,58} J. L. Liu,⁷² J. Y. Liu,^{1,63} K. Liu,¹ K. Y. Liu,⁴¹ Ke Liu,²³ L. Liu,^{71,58} L. C. Liu,⁴⁴ Lu Liu,⁴⁴ M. H. Liu,^{13,f} P. L. Liu,¹ Q. Liu,⁶³ S. B. Liu,^{71,58} T. Liu,^{13,f} W. K. Liu,⁴⁴ W. M. Liu,^{71,58} X. Liu,^{39,j,k} Y. Liu,^{39,j,k} Y. Liu,⁸¹ Y. B. Liu,⁴⁴ Z. A. Liu,^{1,58,63} Z. Q. Liu,⁵⁰ X. C. Lou,^{1,58,63} F. X. Lu,⁵⁹ H. J. Lu,²⁴ J. G. Lu,^{1,58} X. L. Lu,¹ Y. Lu,⁸ Y. P. Lu,^{1,58} Z. H. Lu,^{1,63} C. L. Luo,⁴² M. X. Luo,⁸⁰ T. Luo,^{13,f} X. L. Luo,^{1,58} X. R. Lyu,⁶³ Y. F. Lyu,⁴⁴ F. C. Ma,⁴¹ H. L. Ma,¹ J. L. Ma,^{1,63} L. L. Ma,⁵⁰ M. M. Ma,^{1,63} Q. M. Ma,¹ R. Q. Ma,^{1,63} R. T. Ma,⁶³ X. Y. Ma,^{1,58} Y. Ma,^{47,g} Y. M. Ma,³² F. E. Maas,¹⁹ M. Maggiora,^{74a,74c} S. Malde,⁶⁹ Q. A. Malik,⁷³ A. Mangoni,^{29b} Y. J. Mao,^{47,g} Z. P. Mao,¹ S. Marcello,^{74a,74c} Z. X. Meng,⁶⁶ J. G. Messchendorp,^{14,64} G. Mezzadri,^{30a} H. Miao,^{1,63} T. J. Min,⁴³ R. E. Mitchell,²⁸ X. H. Mo,^{1,58,63} N. Yu. Muchnoi,^{5,b} J. Muskalla,³⁶ Y. Nefedov,³⁷ F. Nerling,^{19,d} I. B. Nikolaev,^{5,b} Z. Ning,^{1,58} S. Nisar,^{12,1} Q. L. Niu,^{39,j,k} W. D. Niu,⁵⁵ Y. Niu,⁵⁰ S. L. Olsen,⁶³ Q. Ouyang,^{1,58,63} S. Pacetti,^{29b,29c} X. Pan,⁵⁵ Y. Pan,⁵⁷ A. Pathak,³⁵ P. Patteri,^{29a} Y. P. Pei,^{71,58} M. Pelizaeus,⁴ H. P. Peng,^{71,58} Y. Y. Peng,^{39,j,k} K. Peters,^{14,d} J. L. Ping,⁴² R. G. Ping,^{1,63} S. Plura,³⁶ V. Prasad,³⁴ F. Z. Qi,¹ H. Qi,^{71,58} H. R. Qi,⁶¹ M. Qi,⁴³ T. Y. Qi,^{13,f} S. Qian,^{1,58} W. B. Qian,⁶³ C. F. Qiao,⁶³ J. J. Qin,⁷² L. Q. Qin,¹⁵ X. P. Qin,^{13,f} X. S. Qin,⁵⁰ Z. H. Qin,^{1,58} J. F. Qiu,¹ S. Q. Qu,⁶¹ C. F. Redmer,³⁶ K. J. Ren,⁴⁰ A. Rivetti,^{74c} M. Rolo,^{74c} G. Rong,^{1,63} Ch. Rosner,¹⁹ S. N. Ruan,⁴⁴ N. Salone,⁴⁵ A. Sarantsev,^{37,c} Y. Schelhaas,³⁶ K. Schoenning,⁷⁵ M. Scodreggio,^{30a,30b} K. Y. Shan,^{13,f} W. Shan,²⁵ X. Y. Shan,^{71,58} J. F. Shangguan,⁵⁵ L. G. Shao,^{1,63} M. Shao,^{71,58} C. P. Shen,^{13,f} H. F. Shen,^{1,63} W. H. Shen,⁶³ X. Y. Shen,^{1,63} B. A. Shi,⁶³ H. C. Shi,^{71,58} J. L. Shi,¹³ J. Y. Shi,¹ Q. Q. Shi,⁵⁵ R. S. Shi,^{1,63} X. Shi,^{1,58} J. J. Song,²⁰ T. Z. Song,⁵⁹ W. M. Song,^{35,1} Y. J. Song,¹³ Y. X. Song,^{47,g} S. Sosio,^{74a,74c} S. Spataro,^{74a,74c} F. Stieler,³⁶ Y. J. Su,⁶³ G. B. Sun,⁷⁶ G. X. Sun,¹ H. Sun,⁶³ H. K. Sun,¹ J. F. Sun,²⁰ K. Sun,⁶¹ L. Sun,⁷⁶ S. S. Sun,^{1,63} T. Sun,^{1,63} W. Y. Sun,³⁵ Y. Sun,¹⁰ Y. J. Sun,^{71,58} Y. Z. Sun,¹ Z. T. Sun,⁵⁰ Y. X. Tan,^{71,58} C. J. Tang,⁵⁴ G. Y. Tang,¹ J. Tang,⁵⁹ Y. A. Tang,⁷⁶ L. Y. Tao,⁷² Q. T. Tao,^{26,h} M. Tat,⁶⁹ J. X. Teng,^{71,58} V. Thoren,⁷⁵ W. H. Tian,⁵⁹ W. H. Tian,⁵² Y. Tian,^{32,63} Z. F. Tian,⁷⁶ I. Uman,^{62b} S. J. Wang,⁵⁰ B. Wang,¹ B. L. Wang,⁶³ Bo Wang,^{71,58} C. W. Wang,⁴³ D. Y. Wang,^{47,g} F. Wang,⁷² H. J. Wang,^{39,j,k} H. P. Wang,^{1,63} J. P. Wang,⁵⁰ K. Wang,^{1,58} L. L. Wang,¹ M. Wang,⁵⁰ Meng Wang,^{1,63} S. Wang,^{13,f} S. Wang,^{39,j,k} T. Wang,^{13,f} T. J. Wang,⁴⁴ W. Wang,⁷² W. Wang,⁵⁹ W. P. Wang,^{71,58} X. Wang,^{47,g} X. F. Wang,^{39,j,k} X. J. Wang,⁴⁰ X. L. Wang,^{13,f} Y. Wang,⁶¹ Y. D. Wang,⁴⁶ Y. F. Wang,^{1,58,63}

Y. H. Wang,⁴⁸ Y. N. Wang,⁴⁶ Y. Q. Wang,¹ Yaqian Wang,^{18,1} Yi Wang,⁶¹ Z. Wang,^{1,58} Z. L. Wang,⁷² Z. Y. Wang,^{1,63} Ziyi Wang,⁶³ D. Wei,⁷⁰ D. H. Wei,¹⁵ F. Weidner,⁶⁸ S. P. Wen,¹ C. W. Wenzel,⁴ U. Wiedner,⁴ G. Wilkinson,⁶⁹ M. Wolke,⁷⁵ L. Wollenberg,⁴ C. Wu,⁴⁰ J. F. Wu,^{1,63} L. H. Wu,¹ L. J. Wu,^{1,63} X. Wu,^{13,f} X. H. Wu,³⁵ Y. Wu,⁷¹ Y. H. Wu,⁵⁵ Y. J. Wu,³² Z. Wu,^{1,58} L. Xia,^{71,58} X. M. Xian,⁴⁰ T. Xiang,^{47,g} D. Xiao,^{39,j,k} G. Y. Xiao,⁴³ S. Y. Xiao,¹ Y. L. Xiao,^{13,f} Z. J. Xiao,⁴² C. Xie,⁴³ X. H. Xie,^{47,g} Y. Xie,⁵⁰ Y. G. Xie,^{1,58} Y. H. Xie,⁷ Z. P. Xie,^{71,58} T. Y. Xing,^{1,63} C. F. Xu,^{1,63} C. J. Xu,⁵⁹ G. F. Xu,¹ H. Y. Xu,⁶⁶ Q. J. Xu,¹⁷ Q. N. Xu,³¹ W. Xu,^{1,63} W. L. Xu,⁶⁶ X. P. Xu,⁵⁵ Y. C. Xu,⁷⁸ Z. P. Xu,⁴³ Z. S. Xu,⁶³ F. Yan,^{13,f} L. Yan,^{13,f} W. B. Yan,^{71,58} W. C. Yan,⁸¹ X. Q. Yan,¹ H. J. Yang,^{51,e} H. L. Yang,³⁵ H. X. Yang,¹ Tao Yang,¹ Y. Yang,^{13,f} Y. F. Yang,⁴⁴ Y. X. Yang,^{1,63} Yifan Yang,^{1,63} Z. W. Yang,^{39,j,k} Z. P. Yao,⁵⁰ M. Ye,^{1,58} M. H. Ye,⁹ J. H. Yin,¹ Z. Y. You,⁵⁹ B. X. Yu,^{1,58,63} C. X. Yu,⁴⁴ G. Yu,^{1,63} J. S. Yu,^{26,h} T. Yu,⁷² X. D. Yu,^{47,g} C. Z. Yuan,^{1,63} L. Yuan,² S. C. Yuan,¹ X. Q. Yuan,¹ Y. Yuan,^{1,63} Z. Y. Yuan,⁵⁹ C. X. Yue,⁴⁰ A. A. Zafar,⁷³ F. R. Zeng,⁵⁰ X. Zeng,^{13,f} Y. Zeng,^{26,h} Y. J. Zeng,^{1,63} X. Y. Zhai,³⁵ Y. C. Zhai,⁵⁰ Y. H. Zhan,⁵⁹ A. Q. Zhang,^{1,63} B. L. Zhang,^{1,63} B. X. Zhang,¹ D. H. Zhang,⁴⁴ G. Y. Zhang,²⁰ H. Zhang,⁷¹ H. C. Zhang,^{1,58,63} H. H. Zhang,⁵⁹ H. H. Zhang,³⁵ H. Q. Zhang,^{1,58,63} H. Y. Zhang,^{1,58} J. Zhang,⁸¹ J. J. Zhang,⁵² J. L. Zhang,²¹ J. Q. Zhang,⁴² J. W. Zhang,^{1,58,63} J. X. Zhang,^{39,j,k} J. Y. Zhang,¹ J. Z. Zhang,^{1,63} Jianyu Zhang,⁶³ Jiawei Zhang,^{1,63} L. M. Zhang,⁶¹ L. Q. Zhang,⁵⁹ Lei Zhang,⁴³ P. Zhang,^{1,63} Q. Y. Zhang,^{40,81} Shuihan Zhang,^{1,63} Shulei Zhang,^{26,h} X. D. Zhang,⁴⁶ X. M. Zhang,¹ X. Y. Zhang,⁵⁰ Xuyan Zhang,⁵⁵ Y. Zhang,⁶⁹ Y. Zhang,⁷² Y. T. Zhang,⁸¹ Y. H. Zhang,^{1,58} Yan Zhang,^{71,58} Yao Zhang,¹ Z. H. Zhang,¹ Z. L. Zhang,³⁵ Z. Y. Zhang,⁴⁴ Z. Y. Zhang,⁷⁶ G. Zhao,¹ J. Zhao,⁴⁰ J. Y. Zhao,^{1,63} J. Z. Zhao,^{1,58} Lei Zhao,^{71,58} Ling Zhao,¹ M. G. Zhao,⁴⁴ S. J. Zhao,⁸¹ Y. B. Zhao,^{1,58} Y. X. Zhao,^{32,63} Z. G. Zhao,^{71,58} A. Zhemchugov,^{37,a} B. Zheng,⁷² J. P. Zheng,^{1,58} W. J. Zheng,^{1,63} Y. H. Zheng,⁶³ B. Zhong,⁴² X. Zhong,⁵⁹ H. Zhou,⁵⁰ L. P. Zhou,^{1,63} X. Zhou,⁷⁶ X. K. Zhou,⁷ X. R. Zhou,^{71,58} X. Y. Zhou,⁴⁰ Y. Z. Zhou,^{13,f} J. Zhu,⁴⁴ K. Zhu,¹ K. J. Zhu,^{1,58,63} L. Zhu,³⁵ L. X. Zhu,⁶³ S. H. Zhu,⁷⁰ S. Q. Zhu,⁴³ T. J. Zhu,^{13,f} W. J. Zhu,^{13,f} Y. C. Zhu,^{71,58} Z. A. Zhu,^{1,63} J. H. Zou,¹ and J. Zu^{71,58}

(BESIII Collaboration)

¹*Institute of High Energy Physics, Beijing 100049, People's Republic of China*

²*Beihang University, Beijing 100191, People's Republic of China*

³*Beijing Institute of Petrochemical Technology, Beijing 102617, People's Republic of China*

⁴*Bochum Ruhr-University, D-44780 Bochum, Germany*

⁵*Budker Institute of Nuclear Physics SB RAS (BINP), Novosibirsk 630090, Russia*

⁶*Carnegie Mellon University, Pittsburgh, Pennsylvania 15213, USA*

⁷*Central China Normal University, Wuhan 430079, People's Republic of China*

⁸*Central South University, Changsha 410083, People's Republic of China*

⁹*China Center of Advanced Science and Technology, Beijing 100190, People's Republic of China*

¹⁰*China University of Geosciences, Wuhan 430074, People's Republic of China*

¹¹*Chung-Ang University, Seoul, 06974, Republic of Korea*

¹²*COMSATS University Islamabad, Lahore Campus, Defence Road, Off Raiwind Road, 54000 Lahore, Pakistan*

¹³*Fudan University, Shanghai 200433, People's Republic of China*

¹⁴*GSI Helmholtzcentre for Heavy Ion Research GmbH, D-64291 Darmstadt, Germany*

¹⁵*Guangxi Normal University, Guilin 541004, People's Republic of China*

¹⁶*Guangxi University, Nanning 530004, People's Republic of China*

¹⁷*Hangzhou Normal University, Hangzhou 310036, People's Republic of China*

¹⁸*Hebei University, Baoding 071002, People's Republic of China*

¹⁹*Helmholtz Institute Mainz, Staudinger Weg 18, D-55099 Mainz, Germany*

²⁰*Henan Normal University, Xinxiang 453007, People's Republic of China*

²¹*Henan University, Kaifeng 475004, People's Republic of China*

²²*Henan University of Science and Technology, Luoyang 471003, People's Republic of China*

²³*Henan University of Technology, Zhengzhou 450001, People's Republic of China*

²⁴*Huangshan College, Huangshan 245000, People's Republic of China*

²⁵*Hunan Normal University, Changsha 410081, People's Republic of China*

²⁶*Hunan University, Changsha 410082, People's Republic of China*

²⁷*Indian Institute of Technology Madras, Chennai 600036, India*

²⁸*Indiana University, Bloomington, Indiana 47405, USA*

^{29a}*INFN Laboratori Nazionali di Frascati, I-00044, Frascati, Italy*

^{29b}*INFN Sezione di Perugia, I-06100, Perugia, Italy*

^{29c}*University of Perugia, I-06100, Perugia, Italy*

^{30a}*INFN Sezione di Ferrara, I-44122, Ferrara, Italy*

^{30b}*University of Ferrara, I-44122, Ferrara, Italy*

³¹*Inner Mongolia University, Hohhot 010021, People's Republic of China*


- ³²*Institute of Modern Physics, Lanzhou 730000, People's Republic of China*
- ³³*Institute of Physics and Technology, Peace Avenue 54B, Ulaanbaatar 13330, Mongolia*
- ³⁴*Instituto de Alta Investigación, Universidad de Tarapacá, Casilla 7D, Arica 1000000, Chile*
- ³⁵*Jilin University, Changchun 130012, People's Republic of China*
- ³⁶*Johannes Gutenberg University of Mainz, Johann-Joachim-Becher-Weg 45, D-55099 Mainz, Germany*
- ³⁷*Joint Institute for Nuclear Research, 141980 Dubna, Moscow region, Russia*
- ³⁸*Justus-Liebig-Universitaet Giessen, II. Physikalisches Institut, Heinrich-Buff-Ring 16, D-35392 Giessen, Germany*
- ³⁹*Lanzhou University, Lanzhou 730000, People's Republic of China*
- ⁴⁰*Liaoning Normal University, Dalian 116029, People's Republic of China*
- ⁴¹*Liaoning University, Shenyang 110036, People's Republic of China*
- ⁴²*Nanjing Normal University, Nanjing 210023, People's Republic of China*
- ⁴³*Nanjing University, Nanjing 210093, People's Republic of China*
- ⁴⁴*Nankai University, Tianjin 300071, People's Republic of China*
- ⁴⁵*National Centre for Nuclear Research, Warsaw 02-093, Poland*
- ⁴⁶*North China Electric Power University, Beijing 102206, People's Republic of China*
- ⁴⁷*Peking University, Beijing 100871, People's Republic of China*
- ⁴⁸*Qufu Normal University, Qufu 273165, People's Republic of China*
- ⁴⁹*Shandong Normal University, Jinan 250014, People's Republic of China*
- ⁵⁰*Shandong University, Jinan 250100, People's Republic of China*
- ⁵¹*Shanghai Jiao Tong University, Shanghai 200240, People's Republic of China*
- ⁵²*Shanxi Normal University, Linfen 041004, People's Republic of China*
- ⁵³*Shanxi University, Taiyuan 030006, People's Republic of China*
- ⁵⁴*Sichuan University, Chengdu 610064, People's Republic of China*
- ⁵⁵*Soochow University, Suzhou 215006, People's Republic of China*
- ⁵⁶*South China Normal University, Guangzhou 510006, People's Republic of China*
- ⁵⁷*Southeast University, Nanjing 211100, People's Republic of China*
- ⁵⁸*State Key Laboratory of Particle Detection and Electronics, Beijing 100049, Hefei 230026, People's Republic of China*
- ⁵⁹*Sun Yat-Sen University, Guangzhou 510275, People's Republic of China*
- ⁶⁰*Suranaree University of Technology, University Avenue 111, Nakhon Ratchasima 30000, Thailand*
- ⁶¹*Tsinghua University, Beijing 100084, People's Republic of China*
- ^{62a}*Turkish Accelerator Center Particle Factory Group, Istinye University, 34010, Istanbul, Turkey*
- ^{62b}*Near East University, Nicosia, North Cyprus, 99138, Mersin 10, Turkey*
- ⁶³*University of Chinese Academy of Sciences, Beijing 100049, People's Republic of China*
- ⁶⁴*University of Groningen, NL-9747 AA Groningen, The Netherlands*
- ⁶⁵*University of Hawaii, Honolulu, Hawaii 96822, USA*
- ⁶⁶*University of Jinan, Jinan 250022, People's Republic of China*
- ⁶⁷*University of Manchester, Oxford Road, Manchester, M13 9PL, United Kingdom*
- ⁶⁸*University of Muenster, Wilhelm-Klemm-Strasse 9, 48149 Muenster, Germany*
- ⁶⁹*University of Oxford, Keble Road, Oxford OX13RH, United Kingdom*
- ⁷⁰*University of Science and Technology Liaoning, Anshan 114051, People's Republic of China*
- ⁷¹*University of Science and Technology of China, Hefei 230026, People's Republic of China*
- ⁷²*University of South China, Hengyang 421001, People's Republic of China*
- ⁷³*University of the Punjab, Lahore-54590, Pakistan*
- ^{74a}*University of Turin and INFN, University of Turin, I-10125, Turin, Italy*
- ^{74b}*University of Eastern Piedmont, I-15121, Alessandria, Italy*
- ^{74c}*INFN, I-10125, Turin, Italy*
- ⁷⁵*Uppsala University, Box 516, SE-75120 Uppsala, Sweden*
- ⁷⁶*Wuhan University, Wuhan 430072, People's Republic of China*
- ⁷⁷*Xinyang Normal University, Xinyang 464000, People's Republic of China*
- ⁷⁸*Yantai University, Yantai 264005, People's Republic of China*
- ⁷⁹*Yunnan University, Kunming 650500, People's Republic of China*
- ⁸⁰*Zhejiang University, Hangzhou 310027, People's Republic of China*
- ⁸¹*Zhengzhou University, Zhengzhou 450001, People's Republic of China*

^aAlso at the Moscow Institute of Physics and Technology, Moscow 141700, Russia.

^bAlso at the Novosibirsk State University, Novosibirsk, 630090, Russia.

^cAlso at the NRC "Kurchatov Institute," PNPI, 188300, Gatchina, Russia.

^dAlso at Goethe University Frankfurt, 60323 Frankfurt am Main, Germany.

 (Received 26 September 2023; accepted 8 January 2024; published 9 February 2024)

Based on a data sample of $(2712.4 \pm 14.3) \times 10^6 \psi(3686)$ events collected with the BESIII detector at the BEPCII collider, the M1 transition $\psi(3686) \rightarrow \gamma \eta_c(2S)$ with $\eta_c(2S) \rightarrow K\bar{K}\pi$ is studied, where $K\bar{K}\pi$ is $K^+K^-\pi^0$ or $K_S^0K^\pm\pi^\mp$. The mass and width of the $\eta_c(2S)$ are measured to be $(3637.8 \pm 0.8(\text{stat}) \pm 0.2(\text{syst})) \text{ MeV}/c^2$ and $(10.5 \pm 1.7(\text{stat}) \pm 3.5(\text{syst})) \text{ MeV}$, respectively. The product branching fraction $\mathcal{B}(\psi(3686) \rightarrow \gamma \eta_c(2S)) \times \mathcal{B}(\eta_c(2S) \rightarrow K\bar{K}\pi)$ is determined to be $(0.97 \pm 0.06(\text{stat}) \pm 0.09(\text{syst})) \times 10^{-5}$. Using $\mathcal{B}(\eta_c(2S) \rightarrow K\bar{K}\pi) = (1.86_{-0.49}^{+0.68})\%$, we obtain the branching fraction of the radiative transition to be $\mathcal{B}(\psi(3686) \rightarrow \gamma \eta_c(2S)) = (5.2 \pm 0.3(\text{stat}) \pm 0.5(\text{syst})_{-1.4}^{+1.9}(\text{extr})) \times 10^{-4}$, where the third uncertainty is due to the quoted $\mathcal{B}(\eta_c(2S) \rightarrow K\bar{K}\pi)$.

DOI: [10.1103/PhysRevD.109.032004](https://doi.org/10.1103/PhysRevD.109.032004)

I. INTRODUCTION

Charmonia, comprising bound states of a charmed quark and its antiquark ($c\bar{c}$), provide a unique opportunity to study the strong interactions in the τ -charm energy regime, where nonperturbative contributions are comparable to perturbative ones. In the low energy region, the large coupling of the strong interaction (α_s) makes first-principle calculations extremely difficult. Thus, various theoretical models have been developed [1–4], and good agreement has been achieved for the mass spectrum of charmonia below the open-charm threshold. However, long-standing puzzles in charmonium physics still exist, such as the $\rho - \pi$ puzzle [5–7] and substantial non- $D\bar{D}$ decays of the $\psi(3770)$ [8,9]. Further studies of the charmonium system are desired, both theoretical and experimental, to resolve

these puzzles and consequently better understand the strong interaction.

The charmonium spin-singlet state $\eta_c(2S)$ was first observed by the Belle collaboration in the B meson decay, $B^\pm \rightarrow K^\pm \eta_c(2S)$, with $\eta_c(2S) \rightarrow K_S^0 K^\pm \pi^\mp$ in 2002 [10]. However, knowledge about this particle is still very limited. For example, the sum of its branching fractions (BFs) measured experimentally is only about 6% [11]. Since the $\eta_c(2S)$ is a pseudoscalar particle with quantum numbers $J^{PC} = 0^{-+}$, it cannot be produced directly via electron-positron annihilation. The production of the $\eta_c(2S)$ through $\psi(3686)$ radiative transition requires a charmed-quark spin flip and, thus, proceeds via a magnetic transition. The partial width $\Gamma(\psi(3686) \rightarrow \gamma \eta_c(2S))$ [1–3] and the BF $\mathcal{B}(\psi(3686) \rightarrow \gamma \eta_c(2S))$ [12] have been calculated in different theoretical frameworks, as shown in Table I. These include the nonrelativistic potential model (NR model) [1,2], the Godfrey-Isgur relativized potential model (GI model) [1,2], the light-front quark model [3], and the other models [12]. Significant discrepancies exist among the predictions.

On the experimental side, the first observation of the M1 transition $\psi(3686) \rightarrow \gamma \eta_c(2S)$ with $\eta_c(2S)$ decaying into $K\bar{K}\pi$ was reported by BESIII [13]. With a data sample of $106 \times 10^6 \psi(3686)$ events, BESIII measured the BF $\mathcal{B}(\psi(3686) \rightarrow \gamma \eta_c(2S)) = (6.8 \pm 1.1 \pm 4.5) \times 10^{-4}$, where, here and hereafter, the first uncertainty is statistical and the second is systematic. The authors of Ref. [7] extracted $\mathcal{B}(\psi(3686) \rightarrow \gamma \eta_c(2S)) = (7_{-2.5}^{+3.4}) \times 10^{-4}$ by a global fit to many experimental measurements and is in good agreement with the world average value of $(7 \pm 5) \times 10^{-4}$ [11]. It is difficult to validate the theoretical calculations with the current measurements, since the relative uncertainties are as large as 70%.

The mass of the $\eta_c(2S)$ was predicted to be 3.630, 3.623, and 3.637 GeV/c^2 according to the NR model [1], the GI model [1], and in Ref. [3], respectively. Recently, the LHCb collaboration reported the mass of the $\eta_c(2S)$ to be $m_{\eta_c(2S)} = (3637.90 \pm 0.54 \pm 1.40) \text{ MeV}/c^2$ and its width to be $\Gamma_{\eta_c(2S)} = (10.77 \pm 1.62 \pm 1.08) \text{ MeV}$, via

^cAlso at Key Laboratory for Particle Physics, Astrophysics and Cosmology, Ministry of Education; Shanghai Key Laboratory for Particle Physics and Cosmology; Institute of Nuclear and Particle Physics, Shanghai 200240, People's Republic of China.

^fAlso at Key Laboratory of Nuclear Physics and Ion-beam Application (MOE) and Institute of Modern Physics, Fudan University, Shanghai 200443, People's Republic of China.

^gAlso at State Key Laboratory of Nuclear Physics and Technology, Peking University, Beijing 100871, People's Republic of China.

^hAlso at School of Physics and Electronics, Hunan University, Changsha 410082, China.

ⁱAlso at Guangdong Provincial Key Laboratory of Nuclear Science, Institute of Quantum Matter, South China Normal University, Guangzhou 510006, China.

^jAlso at Frontiers Science Center for Rare Isotopes, Lanzhou University, Lanzhou 730000, People's Republic of China.

^kAlso at Lanzhou Center for Theoretical Physics, Lanzhou University, Lanzhou 730000, People's Republic of China.

^lAlso at the Department of Mathematical Sciences, IBA, Karachi 75270, Pakistan.

Published by the American Physical Society under the terms of the Creative Commons Attribution 4.0 International license. Further distribution of this work must maintain attribution to the author(s) and the published article's title, journal citation, and DOI. Funded by SCOAP³.

TABLE I. A comparison of theoretical calculations for the $\eta_c(2S)$ mass, the BF $\mathcal{B}(\psi(3686) \rightarrow \gamma\eta_c(2S))$, and the partial width $\Gamma(\psi(3686) \rightarrow \gamma\eta_c(2S))$.

	Mass (MeV/ c^2)	$\mathcal{B}(\psi(3686) \rightarrow \gamma\eta_c(2S))(\times 10^{-4})$	$\Gamma(\psi(3686) \rightarrow \gamma\eta_c(2S))$ (keV)
NR model [1]	3630	7.14 ± 0.19	0.21
GI model [1]	3623	5.80 ± 0.16	0.17
Meson loop correction [2]	N/A	2.72 ± 1.00	0.08 ± 0.03
Light-front quark model [3]	3637	3.9	0.11
Other models [12]	N/A	0.6–36.0	N/A

$B \rightarrow K\eta_c(2S), \eta_c(2S) \rightarrow K_S^0 K\pi$ [14]. The experimental averages of its resonant parameters are $m_{\eta_c(2S)} = (3637.5 \pm 1.1)$ MeV/ c^2 and $\Gamma_{\eta_c(2S)} = (11.3_{-2.9}^{+3.2})$ MeV [11].

The BESIII experiment has collected $(2712.4 \pm 14.3) \times 10^6 \psi(3686)$ events [15], which is 25.5 times larger than the dataset used in the previous measurement [13]. Using this enlarged data sample, we present a comprehensive analysis of the M1 transition $\psi(3686) \rightarrow \gamma\eta_c(2S)$ with $\eta_c(2S)$ decaying into $K\bar{K}\pi$ final states. The resonant parameters of the $\eta_c(2S)$ and the BF of $\psi(3686) \rightarrow \gamma\eta_c(2S)$ are reported with improved precision.

II. DETECTOR AND MONTE CARLO SIMULATION

The BESIII detector [16] records symmetric e^+e^- collisions provided by the BEPCII storage ring [17] in the center-of-mass energy range from 2.0 to 4.95 GeV, with a peak luminosity of 1×10^{33} cm $^{-2}$ s $^{-1}$ achieved at $\sqrt{s} = 3.77$ GeV. BESIII has collected large data samples in this energy region [17]. The cylindrical core of the BESIII detector covers 93% of the full solid angle and consists of a helium-based multilayer drift chamber (MDC), a plastic scintillator time-of-flight system (TOF), and a CsI(Tl) electromagnetic calorimeter (EMC), which are all enclosed in a superconducting solenoid magnet providing a 1.0 T magnetic field. The solenoid is supported by an octagonal flux-return yoke with resistive plate counter muon identification modules interleaved with steel. The charged-particle momentum resolution at 1 GeV/ c is 0.5%, and the dE/dx resolution is 6% for electrons from Bhabha scattering. The EMC measures photon energies with a resolution of 2.5% (5%) at 1 GeV in the barrel (end cap) region. The time resolution in the TOF barrel region is 68 ps, while that in the end cap region is 110 ps. The end cap TOF system was upgraded in 2015 using multigap resistive plate chamber technology, providing a time resolution of 60 ps [18].

Simulated data samples produced with a Geant4-based [19] Monte Carlo (MC) package, which includes the geometric description of the BESIII detector [20] and the detector response, are used to determine the detection efficiencies and to estimate backgrounds. The simulation models the beam energy spread and initial state radiation (ISR) in the e^+e^-

annihilation with the KKMC generator [21]. The inclusive MC sample includes the production of the $\psi(3686)$ resonance, the production of J/ψ via ISR, and the continuum processes incorporated in KKMC. All the known particle decays are modeled with EvtGen [22] using the BFs either taken from the Particle Data Group [11], when available, or otherwise estimated with LUNDCHARM [23]. The final state radiation (FSR) from charged final state particles is incorporated using the PHOTOS package [24]. We generate the $\psi(3686) \rightarrow \gamma\eta_c(2S)$ decay using helicity amplitudes [25] and the $\eta_c(2S) \rightarrow K\bar{K}\pi$ decays with a phase space model.

III. EVENT SELECTION

Here and hereafter, $K\bar{K}\pi$ represents only $K^+K^-\pi^0$ and $K_S^0K^\pm\pi^\mp$ in Secs. III, IV, and V for simplicity except explicitly stated. In selecting signal events for the process $\gamma K_S^0 K^\pm \pi^\mp$, we require each candidate event to contain four charged tracks with zero net charge, and at least one photon; for the $\gamma K^+ K^-\pi^0$ mode, we require each candidate event to contain two charged tracks with zero net charge, and at least three photons. We form $K_S^0(\pi^0)$ candidates using pairs of $\pi^+\pi^-$ ($\gamma\gamma$).

Photon candidates are identified using showers in the EMC. The deposited energy of the shower must be more than 25 MeV in the barrel region ($|\cos\theta| < 0.80$) or more than 50 MeV in the end cap region ($0.86 < |\cos\theta| < 0.92$). To exclude showers that originate from charged tracks, the angle subtended by the EMC shower and the position of the closest charged track at the EMC must be greater than 10 degrees as measured from the interaction point (IP). To suppress the electronic noise and the showers unrelated to the event, the difference between the EMC time and the event start time is required to be within [0, 700] ns.

A charged track is reconstructed from the hits in MDC. We require each charged track not used to reconstruct K_S^0 to satisfy $|\cos\theta| < 0.93$, and the distance of the closest approach to the IP to be within 10 cm along the z axis, and less than 1 cm in the transverse plane. Particle identification (PID) for charged tracks combines measurements of the energy deposited in the MDC (dE/dx) and the flight time in the TOF to form likelihoods $\mathcal{L}(h)(h = p, K, \pi)$ for each hadron h hypothesis. Tracks are identified as K^\pm or π^\pm by comparing the likelihoods for the kaon and

pion hypotheses, requiring $\mathcal{L}(K) > \mathcal{L}(\pi)$ and $\mathcal{L}(\pi) > \mathcal{L}(K)$, respectively.

Each K_S^0 candidate is reconstructed from two oppositely charged tracks which are assigned as $\pi^+\pi^-$ without imposing further PID criteria. They are constrained to originate from a common vertex and are required to have an invariant mass within $|M_{\pi^+\pi^-} - m_{K_S^0}| < 7 \text{ MeV}/c^2$, where $m_{K_S^0}$ is the K_S^0 nominal mass [11]. Here the K_S^0 signal has a mass resolution of $3.5 \text{ MeV}/c^2$. The decay length of the K_S^0 candidate is required to be greater than twice the vertex resolution away from the IP.

For $\gamma K_S^0 K^\pm \pi^\mp$ candidate events, we perform a four-constraint (4C) kinematic fit to all the final state particles with the constraints provided by four-momentum conservation, where the K_S^0 candidate information is from the secondary-vertex fit. We discriminate the $K_S^0 K^+ \pi^-$ and $K_S^0 K^- \pi^+$ charge-conjugate combinations and select the best photon candidate by minimizing $\chi_{\text{com}}^2 = \chi_{4C}^2 + \chi_{\text{PID}}^2(K) + \chi_{\text{PID}}^2(\pi)$, where χ_{4C}^2 is from the 4C kinematic fit. For the $\gamma K^+ K^- \pi^0$ mode, we use a five-constraint (5C) kinematic fit with an additional constraint on the π^0 nominal mass and select the combination with the minimum χ_{5C}^2 . To suppress backgrounds from $\psi(3686) \rightarrow K\bar{K}\pi$ and $\psi(3686) \rightarrow \gamma\gamma K\bar{K}\pi$, we require the χ^2 of the kinematic fit of the $\gamma K\bar{K}\pi$ hypothesis to be less than that from both the $K\bar{K}\pi$ and $\gamma\gamma K\bar{K}\pi$ hypotheses.

IV. BACKGROUNDS ANALYSIS

For the $K_S^0 K^\pm \pi^\mp$ mode, there are significant background contributions from $\psi(3686) \rightarrow \pi^+\pi^- J/\psi$ with J/ψ decaying into e^+e^- and $\mu^+\mu^-$, $\psi(3686) \rightarrow \eta J/\psi$ with η decaying into $\pi^+\pi^-\pi^0$, and from $\psi(3686) \rightarrow \gamma K_S^0 K_S^0$ events with the K^\pm being misidentified as π^\pm . The other backgrounds are from $\psi(3686) \rightarrow \pi^0 J/\psi$ or $\psi(3686) \rightarrow \pi^0 \pi^0 J/\psi$ with J/ψ decaying into e^+e^- , $\mu^+\mu^-$, or K^+K^- , $\psi(3686) \rightarrow \eta J/\psi$ with η decaying into $\gamma\gamma$, $\psi(3686) \rightarrow \omega K^+K^-$ with $\omega \rightarrow \gamma\pi^0 \rightarrow 3\gamma$ for the $K^+K^-\pi^0$ mode. To suppress these backgrounds, we require the recoil mass of any $\pi^+\pi^-$ pair to be less than $3.05 \text{ GeV}/c^2$ to suppress relevant J/ψ backgrounds, and the two charged tracks other than those from the K_S^0 candidate must have an invariant mass differing from $m_{K_S^0}$ by at least $10 \text{ MeV}/c^2$ for $\gamma K_S^0 K_S^0$ backgrounds in the $K_S^0 K^\pm \pi^\mp$ mode. We require the invariant mass of the two charged tracks with μ^\pm hypothesis to be less than $2.90 \text{ GeV}/c^2$ for the $K^+K^-\pi^0$ mode. We suppress the background from $\psi(3686) \rightarrow \omega K^+K^-$, $\omega \rightarrow \gamma\pi^0 \rightarrow 3\gamma$ using an ω veto in the $K^+K^-\pi^0$ mode, i.e., the invariant mass ($M_{3\gamma}$) of the 3γ must satisfy $M_{3\gamma} < 0.74$ or $M_{3\gamma} > 0.82 \text{ GeV}/c^2$. In this case, one γ from ω decays could be misidentified as the radiative photon from $\psi(3686)$ decays.

After imposing the above requirements, the analysis of the inclusive MC sample for $\psi(3686)$ decays with TopoAna [26] indicates that the remaining dominant background sources are: (1) $\psi(3686) \rightarrow K\bar{K}\pi$ events with a fake photon (γ_{fake}) or a photon from FSR in the final state; (2) events with an extra photon, primarily from $\psi(3686) \rightarrow \pi^0 K\bar{K}\pi$ with $\pi^0 \rightarrow \gamma\gamma$; and (3) events from continuum process $e^+e^- \rightarrow \gamma_{\text{ISR}}(\gamma_{\text{FSR}})K\bar{K}\pi$ with the photon from ISR or FSR.

A. $\psi(3686) \rightarrow K\bar{K}\pi$ with a γ_{fake} or FSR

We show the distributions of the invariant mass of $K\bar{K}\pi$ ($M_{K_S^0 K^\pm \pi^\mp}$ and $M_{K^+ K^- \pi^0}$) after the kinematic fits in Fig. 1, where the backgrounds from $\psi(3686) \rightarrow K\bar{K}\pi$ with a γ_{fake} incorporated into the kinematic fit, appear as peaks close to the expected $\eta_c(2S)$ mass, with a sharp cutoff due to the 25-MeV photon-energy threshold. Since the γ_{fake} adds no information to the fit, its inclusion distorts the mass measurement. A modified kinematic fit is therefore imposed by allowing the energy of the photon to float, i.e., using a 3C kinematic fit for $\gamma K_S^0 K^\pm \pi^\mp$ candidates and a 4C kinematic fit for $\gamma K^+ K^- \pi^0$ candidates. We find the

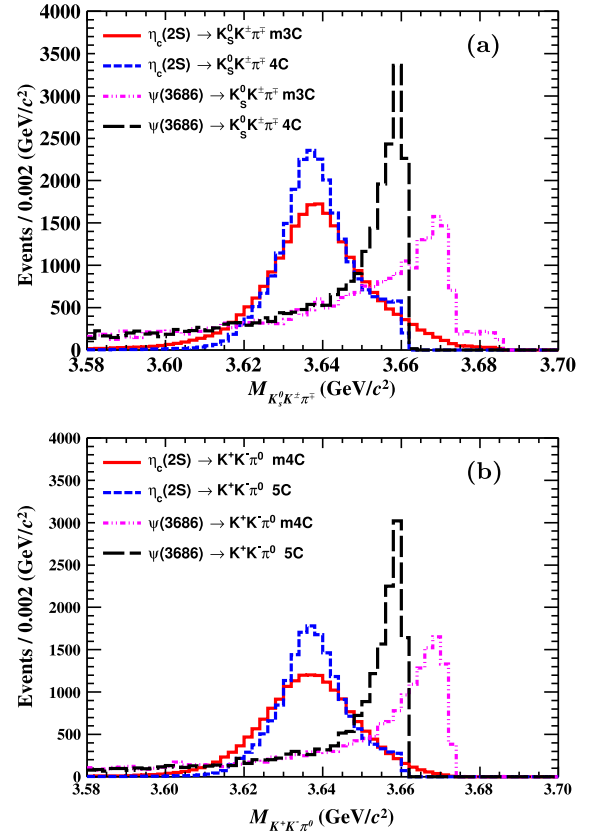


FIG. 1. A comparison between the 4C (5C) and the modified 3C (4C) kinematic fits of the MC samples. (a) and (b) are the invariant mass distributions of $K_S^0 K^\pm \pi^\mp$ and $K^+ K^- \pi^0$ from $\eta_c(2S)$ or $\psi(3686)$ decays, respectively.

energy of the γ from the kinematic fit tends to be zero if it is a fake photon, which is useful for better separating such kinds of backgrounds from the signal. We require the χ^2 in the modified kinematic fits to satisfy $\chi^2_{m3C} < 20$ and $\chi^2_{m4C} < 15$ for the $\gamma K_S^0 K^\pm \pi^\mp$ mode and the $\gamma K^+ K^- \pi^0$ mode, respectively. We use the invariant mass distributions from the modified fits for further study.

The above requirement cannot remove backgrounds from $\psi(3686) \rightarrow K\bar{K}\pi$ with a γ_{FSR} , which could potentially contaminate the signal channel with a long tail in the distribution of $M_{K\bar{K}\pi}$. The contribution depends on the FSR ratio $R_{\text{FSR}} \equiv N_{\text{FSR}}/N_{\text{noFSR}}$ ignoring any dependence on the momentum and angle of the charged tracks, where N_{FSR} and N_{noFSR} are the numbers of events with and without γ_{FSR} , respectively. Control samples of $\psi(3686) \rightarrow \gamma\chi_{c1} \rightarrow \gamma K_S^0 K^\pm \pi^\mp$ (γ_{FSR}) and $\psi(3686) \rightarrow \gamma\chi_{c0} \rightarrow \gamma K^+ K^- K^+ K^-$ (γ_{FSR}) are selected to study the difference of R_{FSR} between data ($R_{\text{FSR}}^{\text{Data}}$) and MC sample ($R_{\text{FSR}}^{\text{MC}}$) in the $\gamma K_S^0 K^\pm \pi^\mp$ and $\gamma K^+ K^- \pi^0$ channels, respectively. We use the same method as described in Ref. [13] to determine $f_{\text{FSR}} \equiv R_{\text{FSR}}^{\text{Data}}/R_{\text{FSR}}^{\text{MC}} = (1.53 \pm 0.05)$ and (1.34 ± 0.12) from two different control samples. We tune the ratio of $\psi(3686) \rightarrow K\bar{K}\pi$ and $\psi(3686) \rightarrow \gamma_{\text{FSR}} K\bar{K}\pi$ in the MC simulation according to f_{FSR} to determine the $M_{K\bar{K}\pi}$ line shape of $\psi(3686) \rightarrow (\gamma_{\text{FSR}}) K\bar{K}\pi$, which will be used to describe the corresponding background contribution in the fit.

B. $\psi(3686) \rightarrow \pi^0 K\bar{K}\pi$

To account for $\psi(3686) \rightarrow \pi^0 K\bar{K}\pi$ backgrounds, we use the same data-driven method as applied in Ref. [13]. We first select $\psi(3686) \rightarrow \pi^0 K\bar{K}\pi$ events in data and then estimate their rate of contamination in the $M_{K\bar{K}\pi}$ spectrum by passing the selected events through the $\gamma K\bar{K}\pi$ selection criteria and correcting with efficiencies determined from MC simulation.

This background contributes a smooth component around the $\chi_{c1,2}$ mass region with a small tail in the $\eta_c(2S)$ signal region that is shown in Fig. 2. We fit these backgrounds with a Novosibirsk function [27], and fix its shape and size in the $M_{K\bar{K}\pi}$ spectra fits.

C. ISR and FSR events from e^+e^- annihilation

We use data collected at $\sqrt{s} = 3.65$ GeV with a luminosity of 401.00 ± 4.01 pb $^{-1}$ [15] to estimate the backgrounds from the continuum processes $e^+e^- \rightarrow \gamma_{\text{FSR}} K\bar{K}\pi$ and $e^+e^- \rightarrow \gamma_{\text{ISR}} K\bar{K}\pi$. After event selection, we shift the mass of $K\bar{K}\pi$ (M_{shifted}) to 3.686 GeV by the rule

$$M_{\text{shifted}} = a \times (M_{K\bar{K}\pi} - m_0) + m_0, \quad (1)$$

where $a = (3.686 - m_0)/(3.65 - m_0)$ with m_0 being the mass threshold for generating $K\bar{K}\pi$. We then normalized the number of continuum backgrounds according to the cross

sections and the integrated luminosities of the data samples at $\sqrt{s} = 3.65$ GeV and at the $\psi(3686)$ peak [15]. We determine the number of continuum events after the selection in the $\psi(3686)$ data sample to be 516 (360) in the $\gamma K_S^0 K^\pm \pi^\mp$ ($\gamma K^+ K^- \pi^0$) final state.

V. BRANCHING FRACTION DETERMINATION

We perform a simultaneous fit to the mass spectra of $K\bar{K}\pi$ in the range of (3.45–3.70) GeV/ c^2 to extract the yield of signal events and the mass and the width of the $\eta_c(2S)$, as shown in Fig. 2. There are χ_{c1} and χ_{c2} signals besides the $\eta_c(2S)$ signals. We use the following line shape of the $\eta_c(2S)$ produced by an M1 transition:

$$(E_\gamma^3 \times \text{BW}(M_{K\bar{K}\pi}) \times f_d(E_\gamma) \times \varepsilon(M_{K\bar{K}\pi})) \otimes \text{DGaus}, \quad (2)$$

where $E_\gamma = (m_{\psi(3686)}^2 - M_{K\bar{K}\pi}^2)/(2m_{\psi(3686)})$ is the energy of the transition photon in the rest frame of the $\psi(3686)$, BW is a Breit-Wigner function with floating width and mean, $f_d(E_\gamma) = E_0^2/(E_\gamma E_0 + (E_\gamma - E_0)^2)$ is a damping function proposed by the KEDR experiment [28] to suppress the diverging tail raised by the term of E_γ^3 with $E_0 = (m_{\psi(3686)}^2 - m_{\eta_c(2S)}^2)/(2m_{\psi(3686)})$ denoting the mean energy of the transition photon, $\varepsilon(M_{K\bar{K}\pi})$ is the efficiency as a fitted polynomial function of $M_{K\bar{K}\pi}$ from the MC simulation, DGaus is a double Gaussian function, i.e. $f \cdot \text{Gaus}(m_1, \sigma_1) + (1 - f) \cdot \text{Gaus}(m_2, \sigma_2)$, which is utilized to describe the resolution. In fact, there are two types of resolutions that need to be taken into account. The first type is based on the detector resolution, which is represented by a double Gaussian function. The parameters of this function are directly determined through MC simulation. The second type of resolution is based on the discrepancy between the data and MC simulation, and is represented by a single Gaussian function. The parameters of this function are obtained through a linear extrapolation from those of $\chi_{c1/2}$. To consider both types of resolutions, a new double Gaussian function, DGaus, is constructed by convoluting the original double Gaussian function with the single Gaussian function. All parameters of DGaus are then determined and fixed during the fitting process.

The line shapes of the $\chi_{c1,2}$ are described with the simulated MC shapes convoluted with a single Gaussian function for the difference in resolution of $M_{K\bar{K}\pi}$ between data and MC simulation, and their parameters are floated in the fit.

We use a Novosibirsk function [27] to parametrize the backgrounds of $\psi(3686) \rightarrow \pi^0 K\bar{K}\pi$ events from data, with the shape of the function and the number of background events fixed. For the background of $\psi(3686) \rightarrow K\bar{K}\pi$ with and without γ_{FSR} , the shape is extracted from MC simulation, with the FSR and non-FSR components reweighted

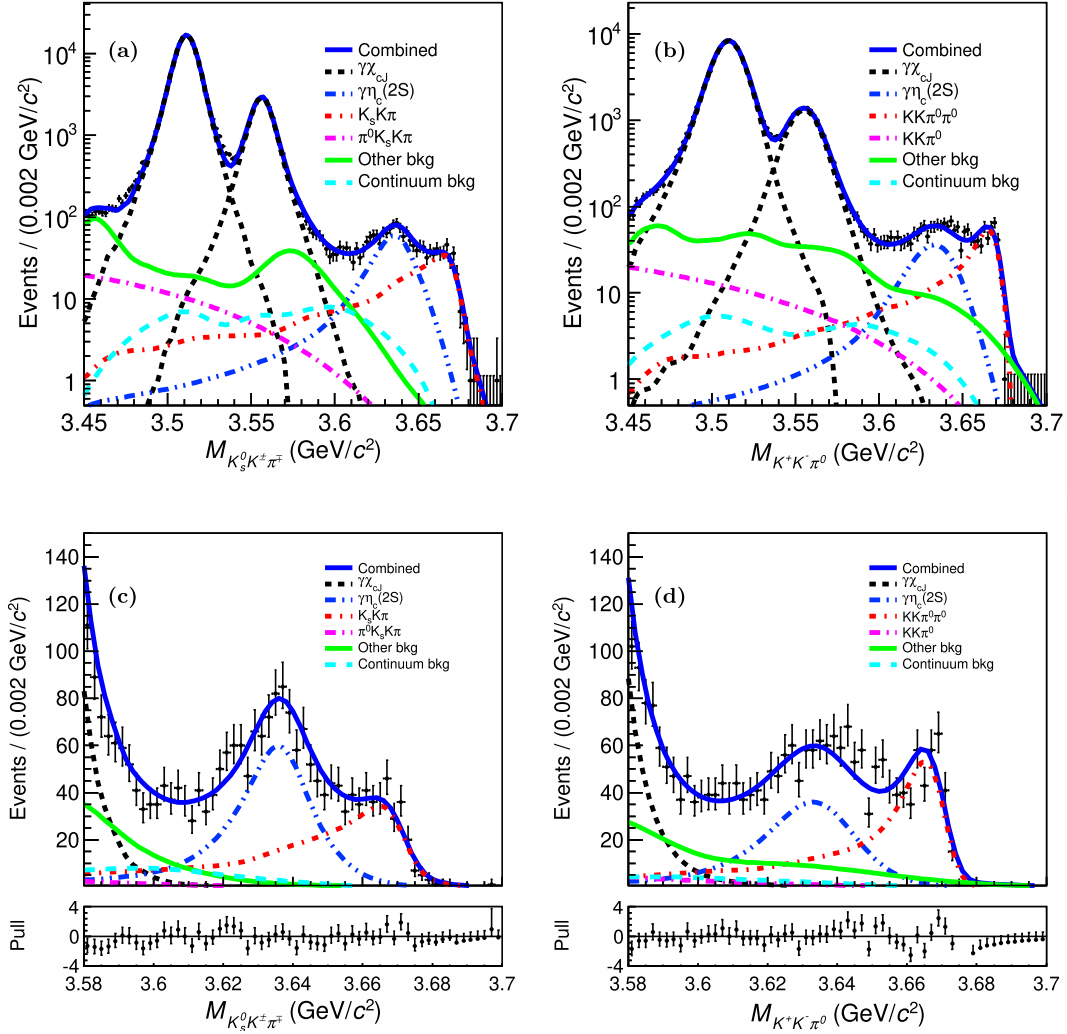


FIG. 2. The distributions of the invariant mass spectra of $K\bar{K}\pi$. The fit results in the whole fit range [(a) and (b)] and in the range only containing $\eta_c(2S)$ signal [(c) and (d)]. Plots (a) and (c) are for the $K_S^0 K^\pm \pi^\mp$ mode, (b) and (d) are for the $K^+ K^- \pi^0$ mode. Dots with error bars are data, blue solid curves are the best results from the simultaneous fits. The blue dashed lines are the $\eta_c(2S)$ signals, and the other dashed lines are backgrounds, among which the pink, red, black, green and cyan ones are from the $\psi(3686) \rightarrow \pi^0 + K\bar{K}\pi$ events, the $\psi(3686) \rightarrow K\bar{K}\pi$ events, the $\psi(3686) \rightarrow \gamma\chi_{c1,2}$ events, other contributions, and continuum contribution, respectively. For plots (a) and (c), the data statistics is summed over the two charge conjugated modes.

by corrected f_{FSR} . We add the continuum backgrounds contribution with shifted mass spectrum shape, and the numbers of continuum backgrounds are fixed. We describe all other smooth backgrounds with the shape fixed to that from the inclusive MC sample while the number of events is floated.

The yields of the $\eta_c(2S)$ signal are 692 ± 42 in the $K^+ K^- \pi^0$ mode and 963 ± 58 in the $K_S^0 K^\pm \pi^\mp$ mode. From the signal MC simulations, we obtain the efficiency $\varepsilon_{K^+ K^- \pi^0} = 16.02\%$ in the $K^+ K^- \pi^0$ mode and $\varepsilon_{K_S^0 K^\pm \pi^\mp} = 15.93\%$ in the $K_S^0 K^\pm \pi^\mp$ mode, respectively. In the MC simulation, the mass and width of the $\eta_c(2S)$ are quoted from the world averaged values [11]. Therefore, we determine the products of the BFs

to be $\mathcal{B}(\psi(3686) \rightarrow \gamma\eta_c(2S)) \times \mathcal{B}(\eta_c(2S) \rightarrow K_S^0 K^+ \pi^- + \text{c.c.}) = (3.23 \pm 0.20) \times 10^{-6}$ and $\mathcal{B}(\psi(3686) \rightarrow \gamma\eta_c(2S)) \times \mathcal{B}(\eta_c(2S) \rightarrow K^+ K^- \pi^0) = (1.61 \pm 0.10) \times 10^{-6}$. The ratio of the BFs agrees well with the isospin symmetry expectation of 2:1 between $K_S^0 K^\pm \pi^\mp$ and $K^+ K^- \pi^0$. We determine the mass and width of the $\eta_c(2S)$ to be $M_{\eta_c(2S)} = (3637.8 \pm 0.8) \text{ MeV}/c^2$ and $\Gamma_{\eta_c(2S)} = (10.5 \pm 1.7) \text{ MeV}$. The uncertainties are statistical only.

Considering isospin conservation, the product BF for $\psi(3686) \rightarrow \gamma\eta_c(2S)$ with $\eta_c(2S) \rightarrow K\bar{K}\pi$ can be obtained by doubling the sum of the $K_S^0 K^\pm \pi^\mp$ and $K^+ K^- \pi^0$ BFs to obtain $\mathcal{B}(\psi(3686) \rightarrow \gamma\eta_c(2S)) \times \mathcal{B}(\eta_c(2S) \rightarrow K\bar{K}\pi) = (0.97 \pm 0.06) \times 10^{-5}$, where the uncertainty takes into account the correlation between the two measured BFs

from the simultaneous fit. Here $K\bar{K}\pi$ indicates the sum of seven channels $K^+K^-\pi^0$, $K_S^0K_S^0\pi^0$, $K_L^0K_L^0\pi^0$, $K_S^0K^+\pi^-$, $K_S^0K^-\pi^+$, $K_L^0K^+\pi^-$, and $K_L^0K^-\pi^+$. If only considering the isospin symmetry, the ratios of the BFs between them should be 2:1:1:2:2:2:2.

VI. SYSTEMATIC UNCERTAINTIES

There are multiple sources of systematic uncertainties in determining the resonant parameters of the $\eta_c(2S)$ and the product of branching fractions $\mathcal{B}(\psi(3686) \rightarrow \gamma\eta_c(2S)) \times \mathcal{B}(\eta_c(2S) \rightarrow K\bar{K}\pi)$.

Systematic uncertainties associated with event selection, such as tracking, PID, photon reconstruction, K_S^0 reconstruction, and kinematic fit are all estimated using control samples. To account for each source's uncertainty, we vary the efficiency accordingly and calculate the difference in the final BF. This difference represents the systematic uncertainty attributed to tracking, PID, and photon reconstruction, respectively. From the study with two control samples, $J/\psi \rightarrow p\bar{p}\pi^+\pi^-$ and $e^+e^- \rightarrow \pi^+\pi^-K^+K^-$, the uncertainties of tracking and PID are 1%, respectively, for each pion and kaon track [29,30]. According to a study with the control sample $J/\psi \rightarrow \rho\pi$, the uncertainty due to photon detection efficiency is 1% per photon and is additive [31]. The systematic uncertainty from the K_S^0 reconstruction is studied using two control samples, $J/\psi \rightarrow K^{*\pm}(892)K^\mp$ with $K^{*\pm}(892) \rightarrow K_S^0\pi^\pm$ and $J/\psi \rightarrow \phi K_S^0K^\pm\pi^\mp$ [32]. We estimate the systematic uncertainty from K_S^0 reconstruction to be 1.2% for the $K_S^0K^\pm\pi^\mp$ mode. To study the uncertainty associated with the kinematic fit, we correct the track helix parameters in the MC simulation [33]. The efficiency

difference 2.8% and 5.1% before and after the correction is taken as the systematic uncertainty related to the kinematic fit for the $K^+K^-\pi^0$ mode and the $K_S^0K^\pm\pi^\mp$ mode, respectively. The resonance parameters of $\eta_c(2S)$ and the intermediate resonances also impact the event selection efficiency. We estimate the systematic uncertainty associated with the resonance parameters of $\eta_c(2S)$ by varying its mass and width by one standard deviation relative to the world average values [11]. Additionally, we consider the influence of intermediate resonances by generating new mixed MC samples with additional decay channels, namely $\eta_c(2S) \rightarrow K_0^*(1430)\bar{K}$ and $\eta_c(2S) \rightarrow K_2^*(1430)\bar{K}$, using fractions inspired by the LHCb study [14]. The difference in efficiency between the new mixed MC samples and the nominal MC samples is taken as the corresponding systematic uncertainty, which is estimated to be 2.9%.

The uncertainties related to the simultaneous fit include those due to the signal resolution function, the efficiency curve, the line shapes of the backgrounds, and the damping function. We estimate the systematic uncertainty due to the resolution function by changing the parameters of the mass and the mass resolution in the single Gaussian function and the convolved double Gaussian function by 1σ . The largest difference is 0.6%, and we take it as the uncertainty due to the resolution function. The uncertainty from the efficiency curve is estimated by comparing the difference in results with and without the efficiency curve. We find a difference of 0.1% and take it as the systematic uncertainty due to the efficiency curve. We estimate the systematic uncertainties due to the line shapes of the backgrounds by using the shapes from alternative ones. The line shape of one background component is changed each time, and the largest

TABLE II. The systematic uncertainty of the $\eta_c(2S)$ mass and width, and the systematic uncertainty of the product BF $\mathcal{B}(\psi(3686) \rightarrow \gamma\eta_c(2S)) \times \mathcal{B}(\eta_c(2S) \rightarrow K\bar{K}\pi)$, represented by $\mathcal{B}\mathcal{B}$ in this Table.

	Source	Mass (MeV/ c^2)	Width (MeV)	$\mathcal{B}\mathcal{B}$ (%)
$K\bar{K}\pi$ event selection	Tracking	2.0
	PID	2.0
	Photon reconstruction	2.7
	Kinematic fit	4.3
	K_S^0 reconstruction	0.8
	Resonance parameters of $\eta_c(2S)$	1.8
	Intermediate resonance	2.9
Simultaneous fit	Resolution function	0.1	0.3	0.6
	Efficiency curve	0.0	0.0	0.1
	Background line shape	0.0	2.9	3.2
	Damping function	0.1	1.9	4.5
	Isospin constraint	0.0	0.1	...
	$\psi(3686)$ data sample	0.5
Number of continuum events	0.0	0.2	1.0	
Shape of continuum		0.1	0.5	2.0
	Combined	0.2	3.5	9.1

TABLE III. A comparison of the experimental measurements in this work with previous BESIII values and world average values for the $\eta_c(2S)$ mass and width, the BF $\mathcal{B}(\psi(3686) \rightarrow \gamma\eta_c(2S))$, and the partial width $\Gamma(\psi(3686) \rightarrow \gamma\eta_c(2S))$.

	Mass (MeV/ c^2)	Width (MeV)	$\mathcal{B}(\psi(3686) \rightarrow \gamma\eta_c(2S))(\times 10^{-4})$	$\Gamma(\psi(3686) \rightarrow \gamma\eta_c(2S))$ (keV)
This work	$3637.8 \pm 0.8 \pm 0.2$	$10.5 \pm 1.7 \pm 3.5$	$5.2 \pm 0.3 \pm 0.5^{+1.9}_{-1.4}$	$0.15^{+0.06}_{-0.04}$
BESIII (2012)	$3637.6 \pm 2.9 \pm 1.6$	$16.9 \pm 6.4 \pm 4.8$	$6.8 \pm 1.1 \pm 4.5$	0.20 ± 0.14
World average	3637.6 ± 1.2	$11.3^{+3.2}_{-2.9}$	7 ± 5	0.21 ± 0.15

difference is used for the uncertainty. We change the relative ratio f_{FSR} by 1σ to evaluate the systematic uncertainty due to FSR. We change the Novosibirsk function to a Gaussian function to estimate the uncertainty due to the shape of the $\pi^0 K \bar{K} \pi$ backgrounds, and change the shape from the inclusive MC sample to the Argus function [34] to estimate the uncertainty due to the shape of other backgrounds. We assume isospin symmetry between $K^+ K^- \pi^0$ and $K_S^0 K^\pm \pi^\mp$ channels in the nominal fit, and take the difference to the result without isospin conservation as the uncertainty associated with the isospin conservation assumption. The systematic uncertainty associated with the damping function is estimated in two ways. One is varying the parameter $m_{\eta_c(2S)}$ by 1σ in KEDR's damping function [28]. The other one is modifying the function from the default KEDR's formula [28] to the alternative CLEO's $\exp(-E_\gamma^2/8\beta^2)$ [35], where $\beta = 0.033$. The maximum differences from the nominal results are taken as the relevant systematic uncertainties.

The uncertainty due to the number of $\psi(3686)$ events in the data sample is determined with inclusive hadronic $\psi(3686)$ decays. The 0.5% is determined to be the systematic uncertainty associated with the number of $\psi(3686)$ events [15].

The uncertainty due to the continuum process includes the number of events and the line shape. We vary the number of continuum events assuming it satisfies a Poisson distribution, and take the difference to the nominal fit result as the corresponding uncertainty. We also vary the smooth parameter of RooKeysPdf [36], which is extracted from the continuum line shape, from 1 to 6, and take the largest difference to the nominal fit result as the corresponding uncertainty.

We summarize the systematic uncertainties in Table II. We assume that all sources of systematic uncertainties are independent and combine them in quadrature to obtain the overall systematic uncertainty.

VII. RESULT AND DISCUSSION

Using a sample of $(2712.4 \pm 14.3) \times 10^6 \psi(3686)$ decays collected by the BESIII detector, we measure the resonant parameters of the $\eta_c(2S)$ and the product

branching fraction $\mathcal{B}(\psi(3686) \rightarrow \gamma\eta_c(2S)) \times \mathcal{B}(\eta_c(2S) \rightarrow K \bar{K} \pi)$ through the hadronic $\eta_c(2S)$ decays $K_S^0 K^\pm \pi^\mp$ and $K^+ K^- \pi^0$ with improved precision. We measure the mass and width of the $\eta_c(2S)$ to be $(3637.8 \pm 0.8 \pm 0.2)$ MeV/ c^2 and $(10.5 \pm 1.7 \pm 3.5)$ MeV, respectively, and $\mathcal{B}(\psi(3686) \rightarrow \gamma\eta_c(2S)) \times \mathcal{B}(\eta_c(2S) \rightarrow K \bar{K} \pi) = (0.97 \pm 0.06 \pm 0.09) \times 10^{-5}$, in which isospin symmetry is assumed. Combining our result with $\mathcal{B}(\eta_c(2S) \rightarrow K \bar{K} \pi) = (1.86^{+0.68}_{-0.49})\%$ [7], we obtain $\mathcal{B}(\psi(3686) \rightarrow \gamma\eta_c(2S)) = (5.2 \pm 0.3 \pm 0.5^{+1.9}_{-1.4}) \times 10^{-4}$, where the last uncertainty is from the quoted $\mathcal{B}(\eta_c(2S) \rightarrow K \bar{K} \pi)$. The partial width $\Gamma(\psi(3686) \rightarrow \gamma\eta_c(2S))$ is also determined to be $0.15^{+0.06}_{-0.04}$ keV by using the total width of the $\psi(3686)$ [11].

Compared with previous measurements [11,13], listed in Table III, our results for the mass and width of the $\eta_c(2S)$ and $\mathcal{B}(\psi(3686) \rightarrow \gamma\eta_c(2S))$ are of comparable precision to the world average values. There is an improvement compared to the previous BESIII result reported in 2012 [13], while the last systematic uncertainty is not significantly reduced due to the large uncertainty of the quoted BF of $\eta_c(2S) \rightarrow K \bar{K} \pi$, which is changed from $1.9 \pm 1.2\%$ [37] to $1.86^{+0.68}_{-0.49}\%$ [7]. Compared with the theoretical calculations [1–3] listed in Table I, our measurement of the partial width $\Gamma(\psi(3686) \rightarrow \gamma\eta_c(2S))$ is consistent with all the theoretical predictions [1–3] within two standard deviations. Therefore, to distinguish various theoretical models, the precision of the experimental measurement needs further improvement. It will be achieved by combining our results to an updated $\mathcal{B}(\eta_c(2S) \rightarrow K \bar{K} \pi)$ that may be obtained via two-photon fusion or B decay processes in the B factories.

ACKNOWLEDGMENTS

The BESIII collaboration thanks the staff of BEPCII and the IHEP computing center for their strong support. This work is supported in part by National Key R&D Program of China under Contracts No. 2020YFA0406301, No. 2020YFA0406300, and No. 2020YFA0406400; National Natural Science Foundation of China (NSFC) under Contracts No. 12275058, No. 11635010, No. 11735014, No. 11835012, No. 11935015, No. 11935016,

No. 11935018, No. 11961141012, No. 12022510, No. 12025502, No. 12035009, No. 12035013, No. 12061131003, No. 12192260, No. 12192261, No. 12192262, No. 12192263, No. 12192264, No. 12192265, No. 12221005, No. 12225509, and No. 12235017; the Chinese Academy of Sciences (CAS) Large-Scale Scientific Facility Program; the CAS Center for Excellence in Particle Physics (CCEPP); Joint Large-Scale Scientific Facility Funds of the NSFC and CAS under Contract No. U1832207; CAS Key Research Program of Frontier Sciences under Contracts No. QYZDJ-SSW-SLH003 and No. QYZDJ-SSW-SLH040; 100 Talents Program of CAS; The Institute of Nuclear and Particle Physics (INPAC) and Shanghai Key Laboratory for Particle Physics and Cosmology; European Union's Horizon 2020 research and innovation program under

Marie Skłodowska-Curie grant agreement under Contract No. 894790; German Research Foundation DFG under Contract No. 455635585, Collaborative Research Center CRC 1044, FOR5327, GRK 2149; Istituto Nazionale di Fisica Nucleare, Italy; Ministry of Development of Turkey under Contract No. DPT2006K-120470; National Research Foundation of Korea under Contract No. NRF-2022R1A2C1092335; National Science and Technology fund of Mongolia; National Science Research and Innovation Fund (NSRF) via the Program Management Unit for Human Resources & Institutional Development, Research and Innovation of Thailand under Contract No. B16F640076; Polish National Science Centre under Contract No. 2019/35/O/ST2/02907; The Swedish Research Council; U.S. Department of Energy under Contract No. DE-FG02-05ER41374.

-
- [1] T. Barnes, S. Godfrey, and E. S. Swanson, *Phys. Rev. D* **72**, 054026 (2005).
- [2] G. Li and Q. Zhao, *Phys. Lett. B* **670**, 55 (2008).
- [3] T. Peng and B. Q. Ma, *Eur. Phys. J. A* **48**, 66 (2012).
- [4] N. Brambilla, S. Eidelman *et al.*, *Eur. Phys. J. C* **71**, 1534 (2011).
- [5] M. Anselmino, M. Genovese, and E. Predazzi, *Phys. Rev. D* **44**, 1597 (1991).
- [6] K. T. Chao, Y. F. Gu, and S. F. Tuan, *Commun. Theor. Phys.* **25**, 471 (1996).
- [7] H. P. Wang and C. Z. Yuan, *Chin. Phys. C* **46**, 071001 (2022).
- [8] M. Ablikim *et al.* (BESIII Collaboration), *Phys. Rev. D* **107**, L091101 (2023).
- [9] Q. Zhao, *Nucl. Phys.* **B207**, 347 (2010).
- [10] S. K. Choi *et al.* (Belle Collaboration), *Phys. Rev. Lett.* **89**, 102001 (2002).
- [11] R. L. Workman *et al.* (Particle Data Group), *Prog. Theor. Exp. Phys.* **2022**, 083C01 (2022).
- [12] K. Gao, arXiv:0909.2812.
- [13] M. Ablikim *et al.* (BESIII Collaboration), *Phys. Rev. Lett.* **109**, 042003 (2012).
- [14] R. Aaij *et al.* (LHCb Collaboration), *Phys. Rev. D* **108**, 032010 (2023).
- [15] M. Ablikim *et al.* (BESIII Collaboration), *Chin. Phys. C* **42**, 023001 (2018). With the same method, the total number of $\psi(3686)$ events collected in 2009, 2012, and 2021 is determined to be 2712.4×10^6 in an uncertainty of 0.5% as a preliminary result. The integrated luminosity of $\psi(3686)$ events is given to be 3877.05 pb^{-1} , and the integrated luminosity of data collected at $\sqrt{s} = 3.65 \text{ GeV}$ in 2022 is measured to be 401.00 pb^{-1} with an uncertainty of 1.0% as a preliminary result.
- [16] M. Ablikim *et al.* (BESIII Collaboration), *Nucl. Instrum. Methods Phys. Res., Sect. A* **614**, 345 (2010).
- [17] M. Ablikim *et al.* (BESIII Collaboration), *Chin. Phys. C* **44**, 040001 (2020).
- [18] X. Li *et al.*, *Radiat. Detect. Technol. Methods* **1**, 13 (2017); Y. X. Guo *et al.*, *Radiat. Detect. Technol. Methods* **1**, 15 (2017); P. Cao *et al.*, *Nucl. Instrum. Methods Phys. Res., Sect. A* **953**, 163053 (2020).
- [19] S. Agostinelli *et al.* (Geant4 Collaboration), *Nucl. Instrum. Methods Phys. Res., Sect. A* **506**, 250 (2003).
- [20] K. X. Huang *et al.*, *Nucl. Sci. Tech.* **33**, 142 (2022).
- [21] S. Jadach, B. F. L. Ward, and Z. Was, *Phys. Rev. D* **63**, 113009 (2001); *Comput. Phys. Commun.* **130**, 260 (2000).
- [22] D. J. Lange, *Nucl. Instrum. Methods Phys. Res., Sect. A* **462**, 152 (2001); R. G. Ping, *Chin. Phys. C* **32**, 599 (2008).
- [23] J. C. Chen, G. S. Huang, X. R. Qi, D. H. Zhang, and Y. S. Zhu, *Phys. Rev. D* **62**, 034003 (2000); R. L. Yang, R. G. Ping, and H. Chen, *Chin. Phys. Lett.* **31**, 061301 (2014).
- [24] E. R. Was, *Phys. Lett. B* **303**, 163 (1993).
- [25] M. Ablikim *et al.* (BESIII Collaboration), *Phys. Rev. D* **106**, 032014 (2022).
- [26] X. Y. Zhou, S. X. Du, G. Li, and C. P. Shen, *Comput. Phys. Commun.* **258**, 107540 (2021).
- [27] H. Ikeda *et al.* (Belle Collaboration), *Nucl. Instrum. Methods Phys. Res., Sect. A* **441**, 401 (2000).
- [28] V. V. Anashin, V. M. Au *et al.*, *Int. J. Mod. Phys. Conf. Ser.* **02**, 188 (2011).
- [29] W. L. Yuan, X. C. Ai, X. B. Ji, S. J. Chen, Y. Zhang, L. H. Wu, L. L. Wang, and Y. Yuan, *Chin. Phys. C* **40**, 026201 (2016).
- [30] M. Ablikim *et al.* (BESIII Collaboration), *Phys. Rev. D* **99**, 091103 (2019).
- [31] M. Ablikim *et al.* (BESIII Collaboration), *Phys. Rev. D* **81**, 052005 (2010).

-
- [32] M. Ablikim *et al.* (BESIII Collaboration), *Phys. Rev. D* **92**, 112008 (2015).
- [33] M. Ablikim *et al.* (BESIII Collaboration), *Phys. Rev. D* **87**, 012002 (2013).
- [34] H. Albrecht *et al.* (ARGUS Collaboration), *Phys. Lett. B* **241**, 278 (1990).
- [35] R. E. Mitchell *et al.* (CLEO Collaboration), *Phys. Rev. Lett.* **102**, 011801 (2009).
- [36] K. S. Cranmer, *Comput. Phys. Commun.* **136**, 198 (2001).
- [37] B. Aubert *et al.* (Belle Collaboration), *Phys. Rev. D* **78**, 012006 (2008).